Available online at www.sciencedirect.com

jmr&t Journal of Materials Research and Technology

journal homepage: www.elsevier.com/locate/jmrt

Original Article

Quantitative analysis of mixed niobium-titanium carbonitride solubility in HSLA steels based on atom probe tomography and electrical resistivity measurements

Johannes Webel [a,*], *Hardy Mohrbacher* [b,c,**], *Eric Detemple* [d], *Dominik Britz* [a], *Frank Mücklich* [a]

[a] *Department of Materials Science, Saarland University, Campus D3.3, Saarbrücken, 66123, Germany*
[b] *NiobelCon Bvba, Schilde, 2970, Belgium*
[c] *Department of Materials Engineering (MTM), KU Leuven, Leuven, 3001, Belgium*
[d] *AG der Dillinger Hüttenwerke, Dillingen, 66763, Germany*

ARTICLE INFO

Article history:
Received 20 December 2021
Accepted 15 March 2022
Available online 22 March 2022

Keywords:
High-strength low-alloy steel
Nb-Ti-Mixed carbonitrides
Solubility
Electrical resistivity measurements
Atom probe tomography

ABSTRACT

Solubility of mixed niobium-titanium carbonitrides in commercially relevant High-Strength Low-Alloy (HSLA) steel was investigated by combined use of electrical resistivity measurements and APT after interrupted quenching from soaking temperatures between 950 and 1250 °C. Increasing electrical resistivity of the bulk material towards higher soaking temperatures was proportional to the nominal niobium addition which was varied between 0.002 and 0.022–0.043–0.085 wt.-%. Correlative APT analysis of the solutes in the steel matrix showed good agreement with electrical resistivity. Investigating numerous precipitate particles, APT also derived a precise composition for mixed niobium-titanium-carbonitrides which constitute the steel microstructure after casting/before soaking. The scavenging of microalloy elements by insoluble titanium nitrides was corrected by means of combined APT analysis of such precipitate and a quantitative image analysis for the estimation of the total volume fraction of titanium nitrides.

For the first time, solute and precipitate composition together were used for solubility calculations of such mixed carbonitrides to derive an experimental solubility product. This was compared to solubility products of well-established simple carbides and nitrides and theoretical calculations of the solubility of multicomponent carbonitrides. The large discrepancy between experimentally derived and modelled solubility emphasizes the necessity of a robust methodology for the quantification of microalloy precipitation in HSLA steels.

* Corresponding author.
** Corresponding author.
E-mail addresses: j.webel@mx.uni-saarland.de (J. Webel), hm@niobelcon.net (H. Mohrbacher).
https://doi.org/10.1016/j.jmrt.2022.03.098

1. Introduction

The controlled dissolution and precipitation of microalloy carbides and nitrides are of crucial importance in many variants of thermo-mechanical steel processing. The dissolution of niobium (Nb) and titanium (Ti) microalloy precipitates typically occurs during soaking treatment at temperatures between 1100 and 1250 °C. It depends on the carbon (C) and nitrogen (N) content whether a microalloy species can be fully dissolved at a given soaking temperature. The composition of precipitates strongly affects their solubility [1]. While TiN is nearly insoluble [2], species of Ti and Nb carbides as well as the respective carbonitrides require a detailed analysis as to what degree they can dissolve at a given soaking temperature. Prior research has revealed that carbonitrides are more temperature-stable than pure carbides. Full dissolution of Nb(C,N) particles [3] requires an austenite temperature being around 130 °C above that necessary for dissolving NbC [4] in a given HSLA steel composition. The formation of pure NbN particles is not likely occurring due to the low nitrogen level in modern HSLA steels. In Nb-Ti dual microalloyed HSLA steels it is common targeting the Ti content to a near-stoichiometric ratio with respect to the residual N level. The stoichiometric Ti:N atomic mass ratio is approximately 3.4. N levels in modern steelmaking range from 30 to 100 mass ppm, which accordingly involves Ti additions in the range of 0.01–0.04 wt.-% in such Nb-Ti microalloy designs.

Complex microalloy compounds can appear as core-shell structures or as randomly mixed particles. The formation of a core-shell structures relies on the early precipitation of TiN particles on which NbC is nucleating and epitaxially growing at a later stage. This mechanism is supported by hot deformation as was outlined by Ma et al. [5]. The chemical composition of particle core and epitaxial layer together with related influencing factors has been described by Craven et al. [6]. Usually, these composite particles have a relatively larger size, ranging from a few ten to several hundred nanometers. Nb involved in such particles does not completely dissolve even during soaking treatments at 1300 °C. The dissolution of an epitaxial NbC layer from a TiN core is retarded due to reduction in the matrix/particle surface area as well as low interfacial energy between core and layer [7]. According to Zhang et al. [8] the interdiffusion of C and N at the interface should result in improved coherency and lower interfacial energy by generating a TiC/NbC interface in favor of a TiN/NbC interface. Consequently, such core-shell particles will tie up part of the added Nb which might not fully redissolve under standard industrial reheating conditions. Thus, part of the added Nb might not be available for deploying its metallurgical effects during or after hot deformation. On the other hand, the scavenged Nb, does not enhance the particle number density available for exerting grain size control during high temperature treatments but rather increases the size of pre-existing TiN particles. In fact, the amount and spatial distribution of these composite particles is fully controlled by the earlier precipitating TiN.

For sub-stoichiometric Ti additions, residual N is available to precipitate as Nb(C,N) whereas super-stoichiometric Ti addition allows forming TiC as well as complex particles such as (Nb,Ti)C or (Nb,Ti)(C,N). These complex compounds have an increased temperature stability [6,9,10] due to the mixing entropy contribution and are therefore less soluble than the simple variants. However, also other alloying elements influence the solubility of microalloy precipitates. It has also been reported that Mn, Mo and Cr increase the solubility of Nb(C,N) whereas Si and Ni decrease it [11–13].

A recent study by the present authors [14] using atom probe tomography on low-carbon steel with various Nb addition levels identified complex precipitates showing a mixed distribution of Nb, Ti, C and N atoms without comprising a core-shell configuration. It is assumed that these Nb-rich particles precipitate at lower austenite temperature involving residual Ti that was not tied up in TiN particles. The spatial distribution of such mixed (Nb,Ti)(C,N) particles is more homogeneous in contrast to the ribbon-like aligned TiN particles typically precipitating in segregation zones towards the end of the solidification stage. Other authors also confirmed a homogenous elemental distribution in mixed (Nb,Ti,V)(C,N) interphase precipitates [15]. Although a mixed (Nb,Ti)(C,N) compound is less stable than a TiN-NbC core-shell particle, it does have an increased temperature stability over that of binary carbides due to a configurational entropy contribution. The configurational entropy contributions from both Ti/Nb mixing, and N deficiency significantly reduce the particle's free energy especially at high temperatures. Hence, such multi-component precipitates could additionally contribute to grain size control under austenite temperatures at which binary compounds (NbC, TiC) are already in the state of dissolution. This contribution is particularly relevant during high temperature slab soaking (1200–1270 °C) or long-time carburizing treatments (980–1050 °C) as well as during welding in the near-fusion line area (1250–1350 °C). It is, thus, desirable to develop a reliable solubility product for such complex compounds.

Different experimental approaches for determining the amount of solute microalloy elements have been used. A popular method is the dissolution of the steel matrix and subsequent chemical extraction of the residual microalloy compounds [16,17]. The comparatively large volume of steel dissolved allows a higher amount of precipitates to be analyzed by transmission electron microscopy (TEM) or X-ray diffraction (XRD) [17] or by inductively-coupled plasma mass spectroscopy (ICP-MS) [16]. The disadvantage of the chemical extraction method is that an unknown proportion of precipitates is lost due to acid attack and during the various stages of centrifugation and filtering [18]. Extraction also has its limits on determining the chemical composition of precipitates. Notable improvement is achieved by the addition of single-particle ICP-MS [19] or the analysis of extracted precipitates in atom probe tomography (APT) [20]. However, those techniques are still experimentally challenging.

The electrical resistivity of the steel matrix is highly sensitive to the content of solute alloying elements, second phases as well as the underlying defect microstructure. This is formulated in Matthiessen's rule, where the different contributions are summed up. Assuming the simplification that dilute solutes are acting as independent scattering centers, the change of resistivity is proportional to the individual element concentrations. The change of electrical resistivity in

steel of identical microstructure allows thus tracing the different dissolution state of precipitates as was shown for Cu [21], C [22] or Nb [14,23–25]. Regarding practical cases, it may be desirable to quantify absolute solute amounts rather than monitoring relative changes in the solute content [22,26]. Atom probe tomography (APT) is a powerful technique for directly measuring the solute content because of its ability to analyze microstructural features with atomic resolution. Performing the APT analysis in a matrix area free of precipitates and atom clusters allows tracing the amount of solute species [14,27–29]. Local variations in the solute content caused by segregation however can disturb the measured result [30,31].

A review by DeArdo [32] suggests that electrical resistivity and APT measurements allow analyzing the solubility behavior of NbC in austenite with relatively high precision. Other techniques tend overestimating the solubility by not taking precipitate size into account or by assuming idealized precipitate compositions and distributions. The present authors recently characterized the progress of strain-induced precipitation of Nb by deriving the amount of solute Nb from electrical resistivity measurements and characterizing precipitate-free regions in the steel matrix by APT [14]. A good correlation between the results of both methods was found.

The aim of the present study is to quantitatively analyze the dissolution behavior of mixed (Nb,Ti)(C,N) precipitates over a range of soaking temperatures from 950 to 1250 °C using the electrical resistivity method. For the alloy variant with the highest Nb addition (0.085 wt.-%), APT was additionally employed to quantitatively characterize the composition of the precipitate population before soaking treatment and to cross-check the amount of solute Nb present in the precipitate-free matrix area of selected temperatures. A calculus correcting the results for the insoluble amount of Nb tied up in initial TiN particles has been implemented as well. The corrected data of solute Nb content over the considered austenite temperature range were then utilized to derive a solubility product for mixed (Nb,Ti)(C,N) particles.

2. Experimental

2.1. Sample production

Laboratory heats of Nb-Ti dual-microalloyed HSLA steels were produced with the alloy compositions shown in Table 1. Those values are the average of each 24 measurements measured by optical emission spectroscopy (OES), where measurement spots were around 2 mm large and 35 mm apart from each other. By keeping the base alloy composition nearly constant, only the Nb microalloy additions were intentionally varied to values of 0.002 (nominally Nb-free), 0.022, 0.042 and 0.085 wt.-% denoted as Nb0+Ti, Nb2+Ti, Nb4+Ti and Nb8+Ti, respectively. Isothermal soaking treatments were performed to dissolve microalloy precipitates present in these steels. Oven temperatures ranged from 1250, 1200, 1150, 1100, 1050 to 950 °C with the intention to produce sample conditions ranging from all precipitates fully dissolved over to fully precipitated. Subsequent APT measurements of respective sample conditions with the highest Nb addition (Nb8+Ti) confirmed full dissolution at 1250 °C, whereas little Nb was left in solution at 950 °C. To mimic the industrial process of slab reheating, sample steel cubes with 30 mm edge length were heated in a chamber oven with a heating rate of roughly 5–6 °C/min to the desired isothermal holding temperature. After holding for 30 min, the sample microstructures were arrested by interrupted quenching in water. Bars of $28 \times 5 \times 5$ mm^3 were machined from the center of the samples.

2.2. Electrical resistivity

Prior to electrical resistivity measurements, the samples were ground up to 1200 grid and deoxidized with citric acid solution to remove any surface contamination. Electrical resistivity of different sample states was derived by placing the steel bars in a DC circuit using a source meter (Keithley 2400) and measuring the voltage drop along the sample using a microvoltmeter (Keithley 2000). Placing the potential points of the voltage measurement connectors 12 mm apart with each connector 6 mm from the bar center, it was assumed to ensure exclusion of outer regions of the steel that was subjected to oxidation or decarburization inside the oven atmosphere. The voltage drop was measured for currents varied between 0 and 1 A in 0.2 A steps at an ambient temperature of 21 ± 0.2 °C. Thermo-electric effects that bias the voltage measurements have been eliminated by voltage summation of inverse current polarities. The resistivity was then calculated from the linear regression of voltage vs current multiplied with the cross-section of the sample bar and divided by the length between the voltage potential points. The cross section is taken as the average multiple of width and length along the sample bar between the potential points measured with a micrometer screw gauge (Mitutoyo, Kawasaki, Japan). The propagated uncertainty of a single resistivity measurement equaled 0.2 nΩm. Each resistivity data point is the average of three individual measurements.

2.3. Atom probe tomography analysis

APT analysis was used for elemental quantification of carbonitride elements Nb, Ti, C, N and V (as impurity) inside

Table 1 – Composition of Nb-Ti dual-microalloy steels.

Sample	C	Si	Mn	P	Cr	Mo	Ni	Cu	Al	N	Nb	Ti
Nb0+Ti	0.044	0.325	1.65	0.012	0.037	0.020	0.200	0.215	0.026	0.005	0.002	0.012
Nb2+Ti	0.047	0.325	1.65	0.013	0.036	0.020	0.200	0.22	0.027	0.005	0.022	0.015
Nb4+Ti	0.047	0.38	1.65	0.013	0.036	0.020	0.220	0.220	0.035	0.005	0.043	0.019
Nb8+Ti	0.042	0.33	1.70	0.013	0.036	0.021	0.195	0.215	0.033	0.006	0.085	0.018

precipitation and it was also exploited for tracing the solute Nb over the range of soaking temperatures to be correlated with the electrical resistivity of the high-Nb steel Nb8+Ti. Field evaporation of steel samples was conducted in a LEAP 3000XHR (Cameca SAS, Gennevilliers, France) using the voltage mode. The details of the technique relying on field-enhanced evaporation of atoms from a sharp sample tip are described elsewhere [33]. Sample tips were prepared from ground (up to 1200 grid paper) and polished (6, 3, 1 μm diamond suspension followed by 0.05 μm silica polishing) samples on random positions. The lift-out technique first described by Thompson et al. was applied with the use of a focused ion beam-equipped scanning electron microscope (FIB-SEM, Helios Nanolab™ 600, Thermo Fisher Inc., Waltham, MA, USA, formerly FEI Company, Hillsboro, OR, USA) [34]. Inside the APT instrument, specimens were cooled down to 60 K in a vacuum (1.36×10^{-11} mbar). Field evaporation of single atoms was achieved by increasing the voltage bias between the sample tip and a local counter electrode in the region of several kV, then ultra-fast pulsing (200 kHz) of the voltage with a pulse-fraction of 15% of the DC voltage was overlaid. The DC voltage was regulated by the instrument to achieve a detection rate of 3 atoms per 1000 pulses. The detected atom sets were analyzed and reconstructed on their respective 3-dimensional position using the commercial software IVAS 3.6.14 (Cameca SAS, Gennevilliers, France). The reconstruction parameters (image compression factor value and tip radius) were varied to match the atomic plane distance which corresponds to the crystallographic information deduced from desorption image of the detected atoms [35]. The solute composition was measured for Nb8+Ti after quenching from the 1250, 1200 °C, 1100 °C as well as 950 °C. Each reported concentration value is the average of each six measurements at two different locations in the steel where each measurement had an atom count N of at least one million atoms. The standard deviation of elemental concentrations C of several individual reconstructions was found to dominate the standard deviation of the atom count, $\sqrt{C \times (1-C)/N}$, of the individual mass spectrum decompositions.

Precipitates were characterized in the as-cast state which is also the basis for slab reheating in the industrial TMPC. The particles were analyzed as defined within an iso-concentration value of 1 at.-% Nb (voxel size 1 × 1x1 nm^3 and delocalization 3 nm in x- and y- and 1.5 nm in z-direction). The small size of the precipitates below 10 nm made it necessary to choose a small iso-concentration value because the reconstruction of the high-field precipitates suffered from local magnification due to large evaporation field differences [36], which made them appear much larger and with a blurred interface. The average composition as well as the composition variation between precipitates within one APT reconstruction and several different reconstructed measurements were analyzed.

2.4. *Correction for precipitating elements tied by insoluble Ti-precipitates*

In the current Nb-Ti dual-microalloyed steels, an *a priori* unknown amount of Nb, C and N may be trapped in insoluble precipitates appearing as larger-sized TiN particles with cube-shaped morphology [10,37]. Electron microscopic images of C replica films (Fig. 1) indicated that those precipitates having sizes in the range of 100 nm are mostly arranged in ribbons along austenite grain boundaries [14] or in former inter-dendritic regions [38]. The analysis of such particles by electron dispersive spectroscopy (EDS) indicates a dominant composition of Ti and participation of Nb in smaller amounts. Randomly distributed TiN particles of about 20 nm diameter having formed inside austenite grains during slow cooling at lower temperatures [39] were only sporadically found in the present samples.

Quantitative image analysis was used for calculating the TiN volume fraction. The relatively large particle size and low

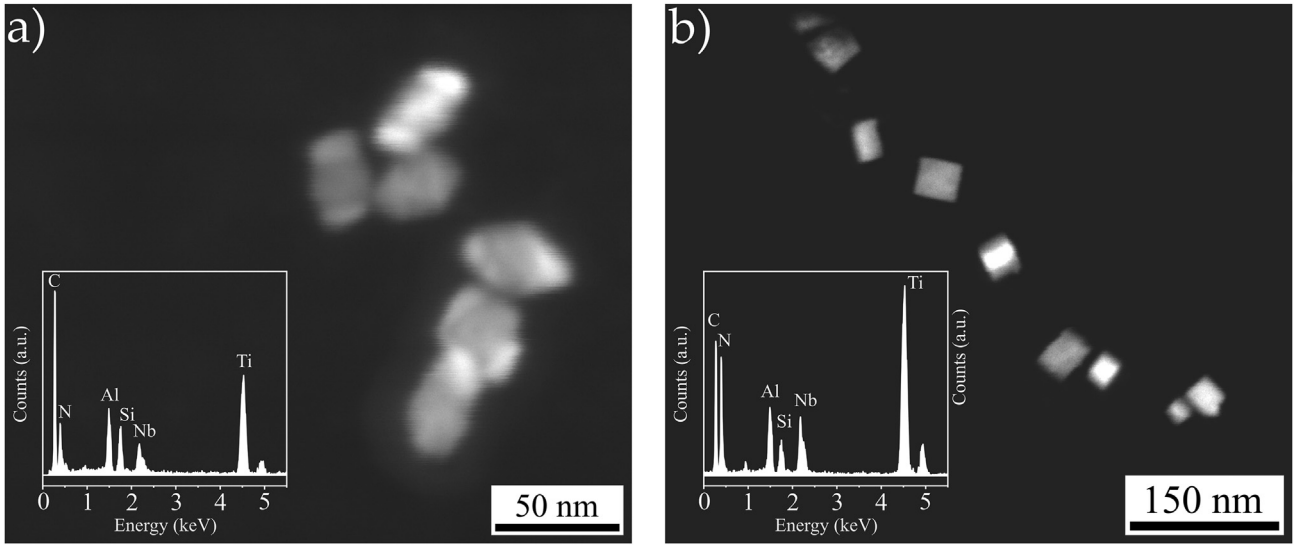

Fig. 1 – C extraction replica TEM micrographs of primarily TiN particles. a) Arrays likely formed during solidification. b) Sporadic presence of heterogeneous NbC grown on TiN core. Some Nb is tied up in both types of precipitates as shown by EDS.

precipitate volume density allowed the use of segmentation being a precise and fast evaluation method. Backscatter electron analysis in the SEM displays the sufficiently large TiN with high elemental contrast against the steel matrix. Steel Nb8+Ti was soaked at 1250 °C and subsequently oxide polished before taking 25 images with a half field width of 8.5 μm in the SEM. These images were hand-segmented in the software package AMIRA (Thermo Fisher Inc., Waltham, MA, USA). Additionally, they were segmented in the free image analysis software FiJi/ImageJ, using the "Trainable WEKA Segmentation" module [40], including one step of pixel erosion around segmented particles. The volume fraction of TiN was then calculated from the average value of all images. This volume fraction was converted into weight fraction of elements that are bound up in the TiN. APT was also used to support this analysis. However, the extremely low particle volume density of TiN did not make random tip specimen preparation a feasible option. A targeted preparation of APT specimen tips containing precipitates in steel was demonstrated in a recent work [20] and adapted here. A TiN particle on the surface was verified by backscattering image contrast in the SEM and marked by FIB patterns before tip preparation.

3. Results

Solubility of (Nb,Ti)(C,N) carbonitrides can be expressed by the composition of the precipitates that exist in equilibrium with the respective solute concentrations in the austenite. In this section, the former is experimentally obtained by APT analysis, and the latter by electrical resistivity measurements with several dissolution states investigated by APT solute composition measurements. For Nb8+Ti, after corrections for competitive precipitation of TiN, a solubility product is calculated from the experimental data.

3.1. *Precipitate composition and size determination by APT*

For Nb8+Ti, APT was used to directly determine the composition of precipitates as well as the matrix by counting the atoms involved. Microalloy carbonitrides are regularly analyzed on their size, shape and composition in high precision [14,28,41–45]. And APT is also feasible for solute content measurements of Nb [14,27,28], C [22,26,46] and N [46–48] in steel. The technique is especially powerful as it is effectively separating precipitate atoms from the steel "matrix", which precipitate-free regions will be called henceforward. The composition is derived from the analysis of the mass spectrum, which is the cumulative count intensity of atom detection events with respect to their flight time, i.e., mass-to-charge state ratio. The specific characteristics of APT mass spectra analysis regarding the quantification of microalloying elements were partly discussed in literature [27,29]. For a detailed listing of the mass spectra analysis focusing on Nb, Ti, C, N inside carbonitrides and in solution the reader is referred to the supporting information.

APT specimens from four different ferrite grains were extracted from the steel in as-cast condition. Approximately 100 small-sized particles of type (Nb,Ti)(C,N) were detected in these samples. These particles were analyzed to determine their exact composition and sizes. Examples of various precipitate populations are shown in Fig. 2.

The measured compositions for 8 reconstruction areas are reported in Table 2. The Nb content in these particles ranges from 36 to 47 at.-% while that of Ti is between 6 and 17 at.-%. The compound has a dominating carbide character as the carbon share is in the range of 40–50 at.-%. The participation of N is with 3–8 at.-% rather small. The respective APT mass spectra contained at least 500 and up to 1500 Nb atoms. Therefore, the variation of element ratios at different reconstruction locations is likely not due to errors related to the peak decomposition, though it must be noted that larger atom count improves the signal-to-noise ratio which affects small isotope peaks, for example of Ti. Larger precipitates appear to tendentially contain relatively more Ti compared to smaller ones (Table 2, reconstruction location 1 and 7, respectively). The average particle composition thus consists of 39 at.-% Nb, 12 at.-% Ti, 43 at.-% C and 6 at.-% N atoms. Using the notation (Nb_xTi_{1-x}) (C_yN_{1-y}), the average particle is defined as $(Nb_{0.76}Ti_{0.24})$ $(C_{0.89}N_{0.11})$. The average Nb:Ti atomic ratio in the precipitates is 3.25. This value is higher than the nominal Nb:Ti ratio in the alloy being 2.5. However, part of the Ti atoms is tied up in insoluble TiN precipitates and is not available for

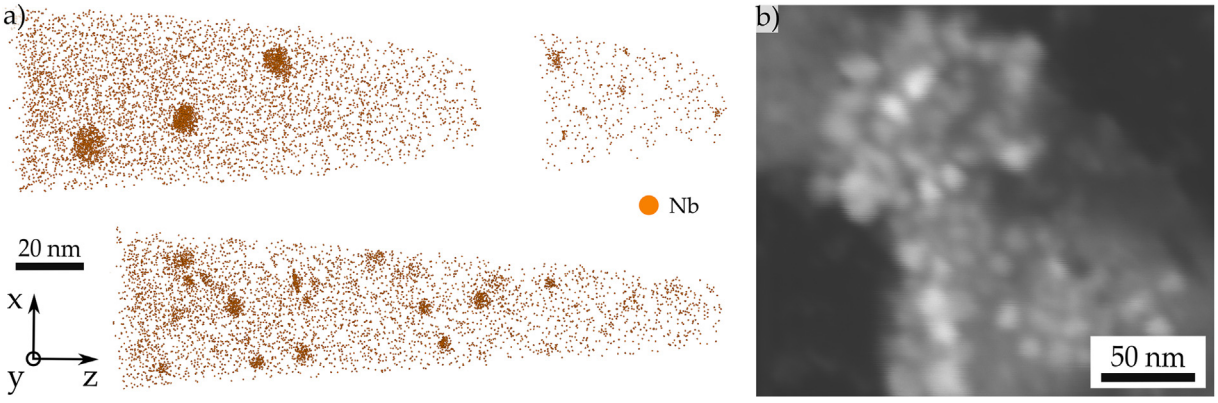

Fig. 2 – (Nb,Ti)(C,N) precipitates in the as-cast condition of Nb8+Ti. a) APT reconstructions of Nb atoms indicating a ranging precipitate size. b) Respective STEM-on-FIB C extraction replica revealing a large amount of approximately <10 nm-sized precipitates.

Table 2 – Atom fractions of elements Nb, Ti, C and N in different APT measurements, and global average over all measurements.

Reconstruction location		1	2	3	4	5	6	7	8
Particle composition (atom fraction)	Nb	0.36	0.36	0.47	0.37	0.42	0.40	0.37	0.39
	Ti	0.14	0.10	0.06	0.12	0.13	0.10	0.17	0.15
	C	0.42	0.50	0.42	0.43	0.40	0.44	0.40	0.42
	N	0.08	0.04	0.05	0.08	0.05	0.05	0.05	0.03
Average particle composition of all measurements (atom fraction)	Nb	0.39			Average atomic Nb/Ti ratio precipitates (APT)			3.25	
	Ti	0.12							
	C	0.43			Nominal atomic Nb/Ti ratio			2.5	
	N	0.06							

participation in the mixed compound. This aspect will be discussed later in more detail.

The particle size cannot be directly determined from the APT reconstruction. The high evaporation field of the precipitates compared to steel matrix leads to the well-described phenomenon of local field magnification [36]. This effect distorts the precipitate-matrix interface inside the APT reconstruction. Accordingly, precipitates like (Nb,Ti)(C,N) with high evaporation field appear larger than they are in reality. Furthermore, interference of atoms segregating from the matrix to the particle-matrix interface complicates the exact definition of the precipitate boundary. The sizes of precipitates shown in Fig. 2a appear to be around 10, 5 and 2 nm. Data obtained from STEM-on-FIB of C extraction replica confirm these sizes (Fig. 2b).

3.2. *Precipitate dissolution characterization*

Microalloy carbonitrides dissolved depending on the austenitization temperature. Precipitate dissolution can be quantified if the solute concentrations of the respective carbonitride elements are known. This was done by electrical resistivity measurements and, in the case of Nb8+Ti, using APT.

3.2.1. *Electrical resistivity*

When carbide and carbonitride precipitates dissolve during soaking treatments the amount of substitutional solute atoms (Nb and Ti) and that of interstitials (C and N) in the matrix increases. Solute atom scattering centers dispersed in the periodic iron lattice increase the electrical resistivity. Between the states of total precipitate dissolution and total precipitation for an identical microstructure and unaltered defect density, the precipitated fraction can be calculated by lever rule. Alternatively, APT allows directly measuring the relative share of solute atoms present in the matrix.

The change in electrical resistivity after different soaking treatments is displayed in Fig. 3 for all investigated alloys. The measured absolute resistivity values in Fig. 3a increase with soaking temperature for all steel compositions. The increase is clearly largest in sample Nb8+Ti. However, the absolute resistivity values do not necessarily correlate with the Nb addition. For instance, sample Nb4+Ti has generally the highest resistivity. This is related to the fact that the Si

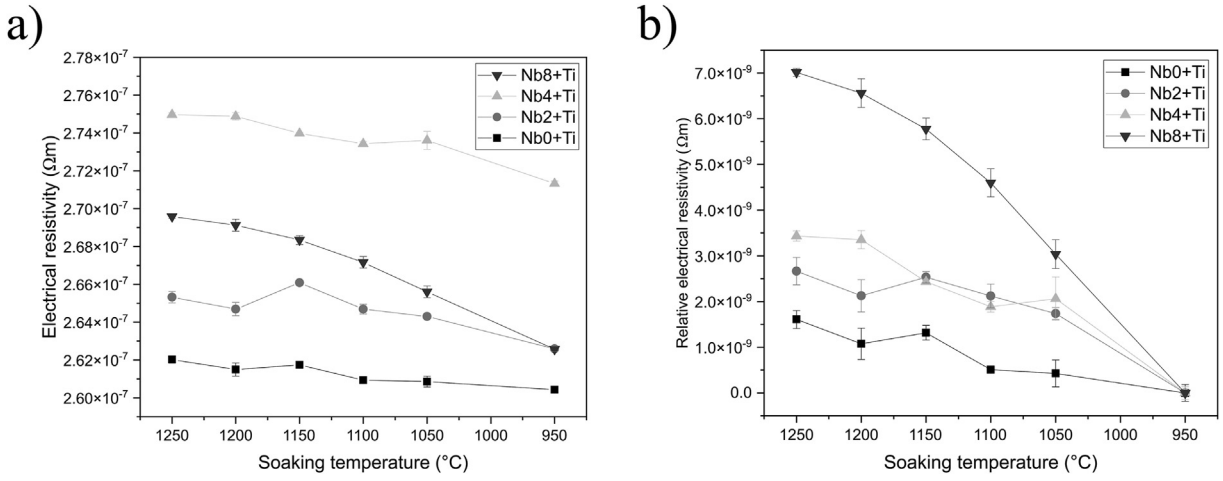

Fig. 3 – Electrical resistivity of Nb0+Ti, Nb2+Ti, Nb4+Ti and Nb8+Ti for various oven soaking treatments over 30 min and supposed full precipitation of Nb. a) absolute resistivity and b) resistivity relative to the supposed fully precipitated conditions.

concentration in sample Nb4+Ti is 0.05 wt.-% higher than in the other samples, and other elements are also contained in higher concentration. Silicon has a strong effect on the resistivity of steels.

The change in resistivity with respect to a reference condition is better suited for the comparison of the carbonitride dissolution of the different Nb grades if it was assumed that in each alloy only the release of carbonitride elements is responsible for the electrical resistivity change. The resistivity of the reference state with supposedly full precipitation (soaking temperature of 950 °C) is subtracted from the resistivities measured after exposure to higher soaking temperatures for each sample material. This relative comparison shown in Fig. 3b reflects the expected behavior according to the added amount of Nb, which supports the assumption that the resistivity increment of the other alloying elements could be treated as a constant and neglected in the later calculations. Compared to 950 °C, all Nb-containing steels had a pronounced increase in electrical resistivity by around 2 nΩm when soaked at 1050 °C. Soaking at 1100 and 1150 °C increases the resistivity only slightly for the Nb2+Ti and Nb4+Ti steels while it continues to increase strongly for the Nb8+Ti steel. After soaking at 1200 °C, Nb8+Ti shows little further increase towards 1250 °C.

The resistivity of the Nb-free steel (Nb0+Ti) changes slightly, with an absolute increase of ≈ 1.5 nΩm between 950 °C and 1250 °C. This increase is surprising as no Nb-related dissolution phenomena can be attributed to it. This is because APT reconstructions found that all elements other than those found in carbonitrides (Fig. 2) remained uniformly distributed and solute concentrations from several APT measurements varied only in the range of the measurement uncertainty. Likewise, on the size scale of the samples made for electrical resistivity measurements, homogeneity of all elements was validated as the elemental concentration was found to be uniform according to OES on multiple locations. In the supporting information, a reasoning is given for different microstructural influences on the resistivity besides the dissolution of the carbonitrides in Fig. 2. It considers lattice defects, competitive dissolution of Ti and the behavior of C during quenching. Comparison of Nb-Ti steels with Ti-free Nb steels and XRD analysis discarded the influences of Ti dissolution or a pronounced effect of lattice defects on the electrical resistivity, in contrast to other work [21–23,25]. In conclusion, carbon-related effects caused by auto-tempering were thought to be the most likely reason for a slight increase of electrical resistivity towards higher austenitizing temperatures.

Comparing the currently analyzed steels to Ti-free steels, it was assumed that these effects are similar for the other Nb-levels as well. Hence, this inherent behavior of the resistivity increment (baseline) not being related to Nb (or Ti) precipitation, was subtracted from the other curves giving the result shown in Fig. 4a.

3.2.2. *APT solute measurements*

The solute Nb concentration in the matrix measured by APT data for soaking temperatures of 1250, 1200, 1100 and 950 °C of Nb8+Ti is overlaid with the electrical resistivity (Fig. 4b). After soaking at 1250 °C, the total amount of solute Nb is determined to be 0.083 ± 0.002 wt.-%. With the nominal Nb composition being 0.085 wt.-% this status can be considered as fully dissolved (the fraction of Nb trapped inside TiN will be discussed below). The APT data indicate that only 0.008 wt.-% Nb were in solution after soaking at 950 °C. This can be considered as nearly complete precipitation. It should be noted, however, that a small amount of residual solute Nb was consistently measured in all investigated areas. A deviation between the electrical resistivity and APT methods is most pronounced after soaking at 1100 °C. A possible explanation for this deviation will be discussed later. The APT data indicate that after soaking at 1200 °C 0.077 wt.-% Nb is dissolved while after soaking at 1100 °C only about half of the nominal Nb concentration is in solution (0.044 wt.-%).

APT found a concentration of Ti of 0.007 ± 0.002 wt.-% in solution after soaking at 1250 °C which is lower than the nominal addition. Part of Ti might be missed in the 24 Da peak

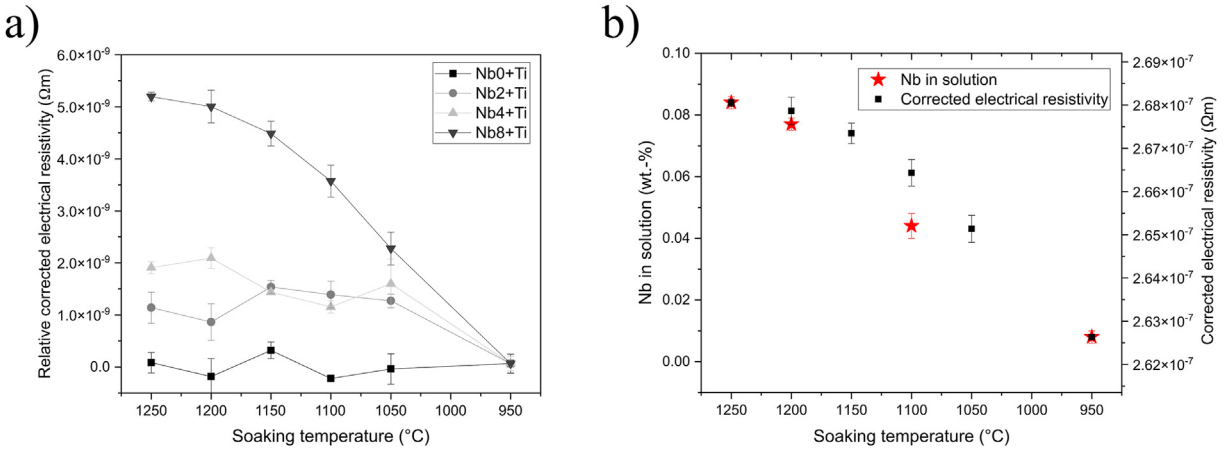

Fig. 4 – a) Nb0+Ti-baseline-corrected relative electrical resistivity and b) Nb0+Ti-baseline-corrected electrical resistivity of Nb8+Ti and solute Nb concentrations (APT) for Nb8+Ti at different temperatures (the values of both data sets were scaled to match at the lowest and highest temperature for facilitating comparison).

which is attributed to C_2^+ due to low ion count. It is also reasonable to expect a considerable share of Ti to be tied up in insoluble TiN-precipitates even at 1250 °C which will be discussed further below.

The average C concentration at 1250 °C is affected by a large statistical error (0.049 ± 0.006 wt.-%) which is primarily related to inhomogeneous distribution of C atoms within the microstructure in combination with the extremely small sampling volume investigated in APT. Carbon in steel quenched from austenite typically segregates to prior austenite grain boundaries, lath boundaries or dislocations [20,49].

For N, a level of around 0.0035 ± 0.001 wt.-% was derived from the NbN peaks (NbN^{3+} at 35.7 Da and NbN^{2+} 53.5 Da). This is in relatively good agreement with the nominal concentration (0.005 wt.-%) considering the error margin and that some *a priori* unknown fraction of N is tied up in stable TiN precipitates.

3.3. Calculation of temperature-dependent solute concentrations

3.3.1. Mass balances of solute Ti, C, N

Solute concentrations of other carbonitride elements were calculated from the amount of solute Nb previously characterized. This was based on the assumption that the dissolution of (Nb,Ti)(C,N) precipitates released on average the amount of Ti, C and N in proportion to the amount of Nb inside the precipitates. The atomic fractions $\chi_{i,ppt}$ of the elements i = Nb, Ti, C, N in the precipitates as characterized by APT and respective nominal concentrations from melt analysis (subscript N) lead to the following mass balances:

$$[C] = ([C]_N - 12/93 \bullet ([Nb]_N - [Nb])) \bullet \chi_{C,ppt}/\chi_{Nb,ppt} \quad (1a)$$

$$[N] = ([N]_N - 14/93 \bullet ([Nb]_N - [Nb])) \bullet \chi_{N,ppt}/\chi_{Nb,ppt} \quad (1b)$$

$$[Ti] = ([Ti]_N - 48/93 \bullet ([Nb]_N - [Nb])) \bullet \chi_{Ti,ppt}/\chi_{Nb,ppt} \quad (1c)$$

where [Nb, C, N, Ti] are the respective actual solute concentrations. The factors 12, 14, 48 and 93 refer to the atomic weights of C, N, Ti and Nb, which are used here to scale the atomic fractions to weight fractions.

3.3.2. Solute amount correction related to insoluble TiN

As mentioned before, carbonitride solubility based on concentrations derived from Eq. (1a-c) is overestimated as precipitation of TiN withdraws a certain amount of mainly Ti and N, but possibly also involves some Nb and C. Zou and Kirkaldy [39] pointed out that large TiN particles do not form an equilibrium with the smaller Ti-containing precipitates, such that their solubility depends only on the remaining solutes in austenite.

Values deduced from Eq. (1a-c) can therefore be corrected by the amount of Nb, Ti, C and N that are tied up in large TiN particles formed during slow cooling of the cast after solidification [50]. These particles having sizes of around 100 nm are quite easily visible in the backscatter contrast of SEM (Fig. 5a). The linear array of precipitates decorates prior austenite grain boundaries as was also observed in carbon replica studies performed in a previous study on the same steels (Fig. 1) [14].

The volume fraction of TiN was estimated by quantitative image analysis of a stack of 25 segmented images like Fig. 5b according to:

$$V_V = V_A = \sum_{i=1}^{25} \frac{A_{TiN,i}}{A_{tot,i}}, \quad (2)$$

Here, V_V is the volume fraction, A_V is the area fraction, A_{TiN} is the area of segmented TiN (white color in Fig. 5b) and A_{tot} is the total image area. The analysis revealed the TiN fraction being V_V = 0.015 ± 0.002% and 0.018 ± 0.003% for hand- and machine-learned segmentation, respectively. The volume fraction is converted into fractions of the individual precipitate forming elements by using the composition of TiN precipitates determined by APT. A particle encapsulation technique applicable to FIB-and-APT preparation [20] allowed the partial atomic reconstruction of a TiN precipitate (Fig. 5d). The straight interface is originating from a cube face of the particle. Besides Ti and N, the particle also contains Nb and small amounts of C. With atomic fractions of 48.5 and 41.9% for Ti and N, these elements form the bulk of the analyzed precipitate. Nb and C participate in this particle with 6.6 and 3.0%, respectively. Conversion into mass fraction amounts to 65.3, 16.5, 17.2 and 1% for Ti, N, Nb and C, respectively.

Assuming the analyzed composition being valid for all TiN particles present in the steel and considering the TiN volume fraction determined by manual segmentation, the corrected solute amounts of Ti, N, Nb and C are decreased by 60, 15, 20 and below 10 mass ppm, respectively. Relative to the nominal concentrations of each element, the TiN particles trap minor amounts of Nb and C. In Table 3, the bulk alloy composition corrected by the fraction bound in TiN is compared to the actual solute concentrations found in APT at the highest temperature. Nb, C and N show excellent agreement whereas Ti is lower in APT which was discussed above. The corrected bulk atomic Nb:Ti ratio is 3.72, which is closer to the average Nb:Ti ratio inside the precipitates being 3.25 (Table 2). The comparison however suggests that some Nb should exist in a different compound.

Using the corrected nominal amounts in Eq. (1) and taking the solute amount of Nb determined from the electrical resistivity after the different soaking treatments allows calculating the solute amounts for all other elements (Fig. 6).

3.4. (Nb,Ti)(C,N) solubility calculations using solute and precipitate compositions

With the knowledge of average (Nb,Ti)(C,N) precipitate composition and the temperature-dependent solute concentrations of Nb, Ti, C and N, the carbonitride solubility in austenite was calculated. The reaction formula of precipitate formation is:

$$Nb_{0.76}Ti_{0.24}C_{0.89}N_{0.11} \Leftrightarrow 0.76 \cdot [Nb] + 0.24 \cdot [Ti] + 0.89 \cdot [C] + 0.11 \cdot [N] \quad (3)$$

The ratio of activities, *a*, of elements being in solution and tied up in precipitates is represented by an equilibrium constant, *K*, which is proportional to the Gibbs free enthalpy of precipitate solution, ΔG^0_{sol}, and the temperature, *T*, as:

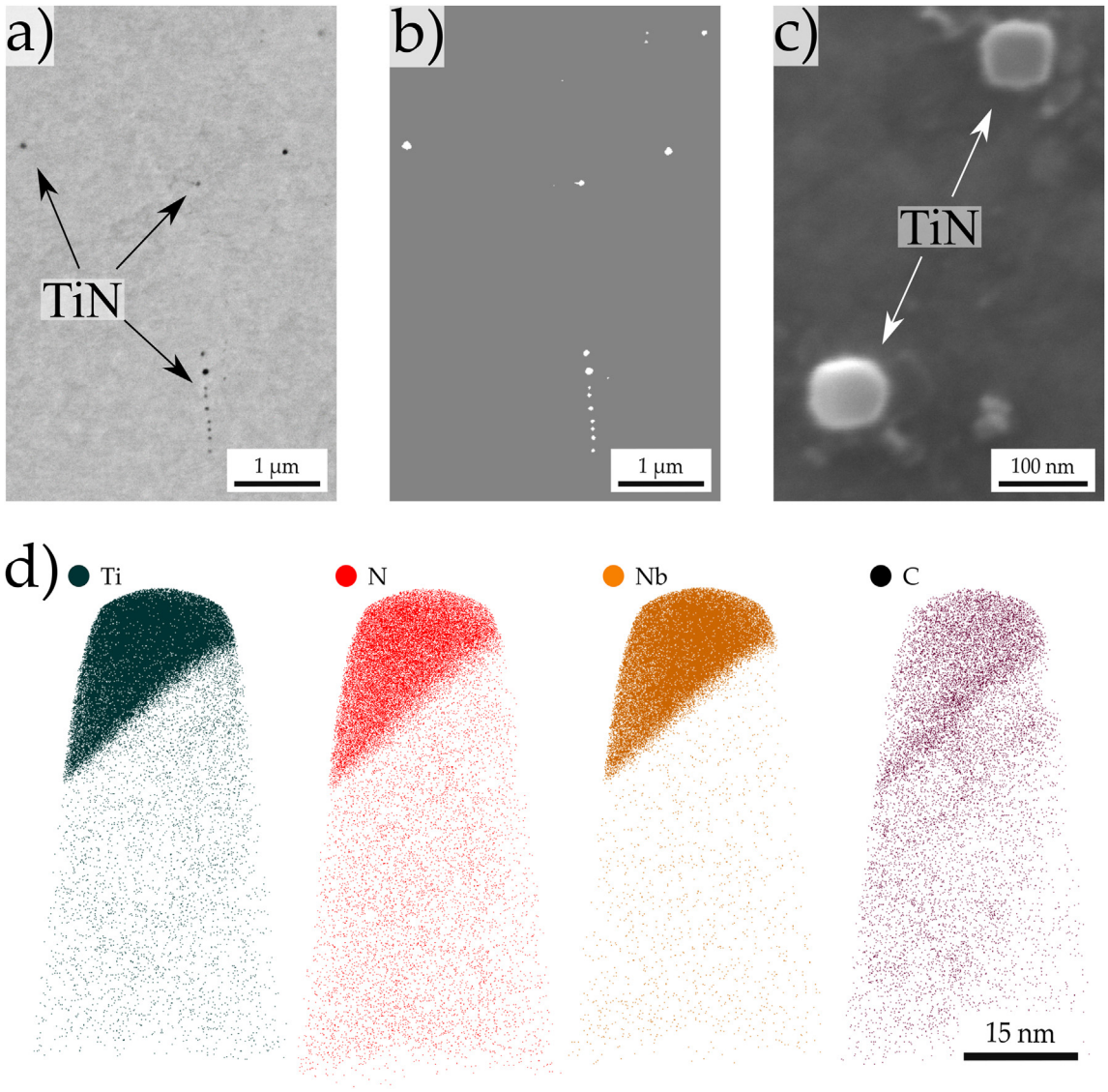

Fig. 5 – a) Backscatter contrast image in SEM showing TiN precipitates which often are aligned in linear arrays, b) segmented image (with precipitates labelled with white color. c) SEM image of TiN after employing etching for the use of the site-specific APT methodology described in [20], which allowed APT analysis of a single TiN. d) Atom maps of Ti, N, Nb and C (descending atomic concentration) of a partial reconstruction of a TiN.

Table 3 – Comparison of bulk solute concentrations corrected for elements trapped in TiN and actual concentrations analyzed with APT for the Nb8+Ti steel after soaking at 1250 °C.

Element	Corrected bulk wt.-% based on electrical resistivity	Solute wt.-% after soaking at 1250 °C based on by APT analysis
Nb	0.083	0.083 ± 0.002
Ti	0.0115	0.007 ± 0.002
C	0.042	0.049 ± 0.006
N	0.0035	0.003 ± 0.001

$$K = \frac{a_{Nb}^{0.76} a_{Ti}^{0.24} a_{C}^{0.89} a_{N}^{0.11}}{a_{Nb_{0.76}Ti_{0.23}C_{0.89}N_{0.11}}} \propto \exp\left(\frac{-\Delta G^{0}_{sol}}{RT}\right). \quad (4)$$

Eq. (4) is used assuming that the composition of the dissolving carbonitride remained constant at each dissolution temperature. Other researchers pointed out that the carbonitride composition is affected strongly by the steel composition and less by the dissolution temperature [1,9]. With the activity of the precipitate being unity and the elemental activities in this dilute system depend on their concentrations, K can be expressed as the solubility product in the well-known form:

$$\lg K = \lg\left([Nb]^{0.76}[Ti]^{0.24}[C]^{0.89}[N]^{0.11}\right) = A - \frac{B}{T}, \quad (5)$$

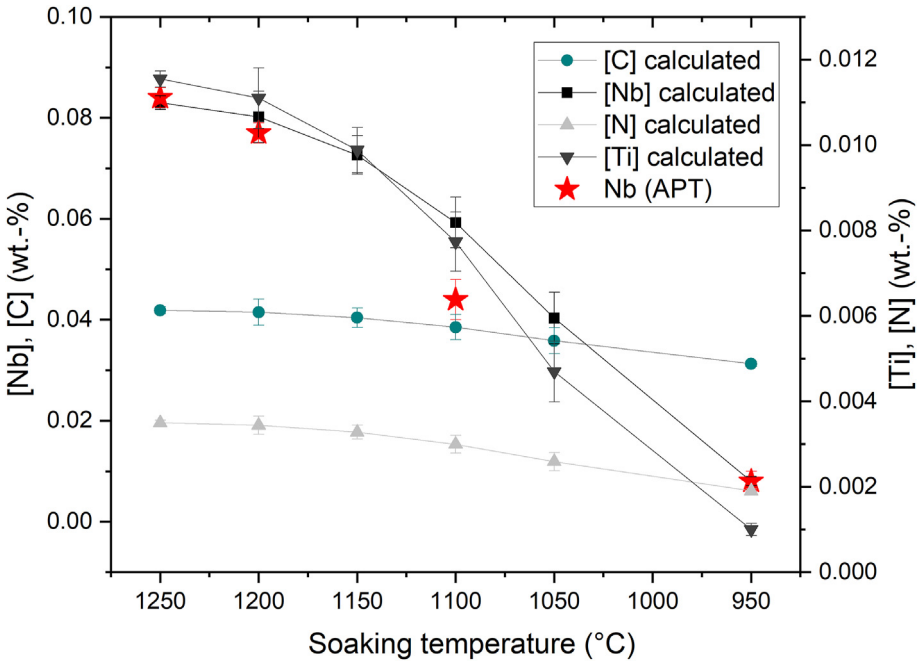

Fig. 6 – Concentration of solute elements derived from Nb concentration measurements by electrical resistivity in alloy Nb8+Ti according to eqs. (1a-c). The average particle composition was determined by APT and all values are corrected for elements trapped in TiN particles.

where the constants A and B include the activity coefficients of the respective elements and the enthalpy ΔG^0_{sol}. Using the solute concentration calculated from the electrical resistivity measurements (Fig. 6), lg *K* is plotted against the inverse absolute temperature in Fig. 7. Two limiting temperatures must be accounted for. Above 1200 °C, this steel can dissolve more Nb than actually added in the Nb8+Ti alloy. Thus, the experimentally determined data point at 1250 °C is omitted in the linear regression fitting. On the other hand, at 950 °C the solute concentration of Nb and Ti is so small that the solubility product is largely disturbed by the measurement error (Table 4). The linear regression of the remaining data points in the range of 1200 to 1050 °C yields the following solubility product:

$$\lg K = 0.33 - 4577/T \text{ with coefficient of determination } R^2 = 0.93. \quad (6)$$

If despite the high error margin, the solubility calculated from electrical resistivity at 950 °C was considered in the linear regression analysis, the solubility product would be:

$$\lg K = 1.06 - 5621/T,\ R^2 = 0.86. \quad (7)$$

In the subsequent considerations, however, rather the solubility product defined by Eq. (6) will be used. This equation is generally in good agreement with the solute Nb concentrations measured by the APT method. For 1250 °C the equation predicts complete Nb dissolution which is experimentally confirmed. The potential origin of the rather large discrepancy at 1100 °C between the prediction by Eq. (6) and the measurement by the electrical resistivity method will be discussed in section 4.2.

4. Discussion

The solubility of binary NbC and NbN compounds using established equations by Narita [4] were calculated for the effective Nb, C and N contents, i.e., the nominal concentrations corrected by the amounts tied up in insoluble TiN particles. The comparison in Fig. 7 indicates that the experimentally derived solubility of the complex carbonitride originating from the current study lies between those of the binary compounds. A transition of the dissolution behavior being closer to that of NbC at lower soaking temperature towards one close to NbN at higher soaking temperatures is observed.

All precipitates investigated (Fig. 2a and Table 2) appeared to have an initially homogeneous distribution of Nb, Ti, C and N as far as the spatial resolution of the APT method could reveal. Core-shell type particles with Nb-rich phases epitaxially grown on Ti-rich cores were only sporadically observed (see Fig. 1a). It can therefore be concluded that mutual solubility of the simple carbides and nitrides appears possible even to a high fraction of atomic exchange of both substitutional and interstitial sites in the fcc NbC superlattice.

4.1. *Comparison of experimentally derived solubility with model calculations*

With the assumption of ideal solution, the solubility of the complex carbide is proportional to the activity of the elements, and thus in diluted state proportional to their fractions. The following expression for a solubility product based

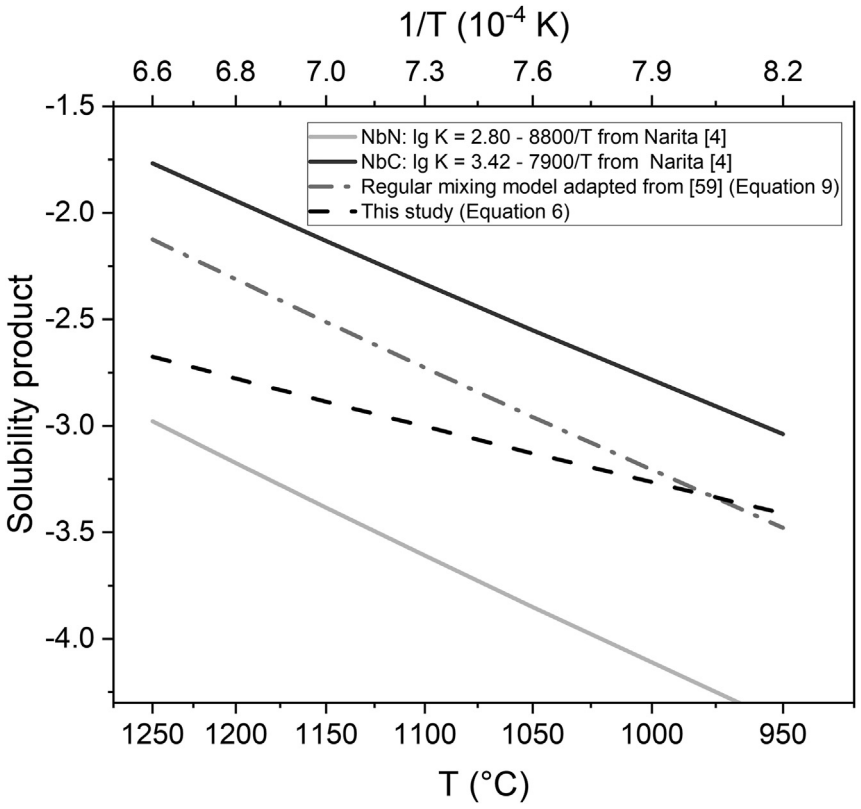

Fig. 7 – Temperature dependence of the solubility product for $Nb_{0.76}Ti_{0.24}C_{0.89}N_{0.11}$ as present in the Nb8+Ti alloy of this study. The line is the linear fit to data in Table 4 (Eq. (6)). Solubility products of binary NbC and NbN according to Narita [4] are indicated for reference. The solubility product assuming regular mixing [51] is calculated as a linear combination of simple carbide and nitride solubilities for the current Nb-Ti precipitate composition (Eq. (9)).

on ideal mixing of the involved species was adapted from Zou and Kirkaldy [51]:

$$\begin{aligned} \lg K = {} & x(1-y)\lg K_1 + xy\lg K_2 + (1-x)(1-y)\lg K_3 + (1-x)y\lg K_4 \\ & + x\lg x + (1-x)\lg(1-x) + y\lg y + (1-y)\lg(1-y) \\ & + \frac{\Omega}{RT\ln 10}(y-y^2) + \frac{4\sigma V_c}{rRT\ln 10}, \end{aligned} \tag{8}$$

with x and y being the fraction of Nb and C and K_1, K_2, K_3 and K_4 being the solubility products of NbN, NbC, TiN and TiC. The regular solution parameter Ω is assumed having an identical value of −4260 J/mol for the interactions of both, Nb and Ti, with C and N (C and N interactions are taken to be zero according to [52]). The latter energy term refers to the solubility of a carbonitride due to the particle/austenite interface (Gibbs-Thompson effect) which increases with decreasing particle radius r and increasing interfacial energy σ. Here, an average particle radius of 2.5 nm was taken for the (Nb,Ti)(C,N) particle population based on the current measurements. A value of $\sigma = 0.3$ J/m^2 was chosen for the interfacial energy, reasonably in agreement with those used in modelling [53,54]. The molar volume of the carbonitrides is calculated as $V_c = 1.3 \times 10^{-5}$ m^3/mol from the known APT composition of precipitates, assuming the lattice parameters of the binary phases to sum up proportionally to their fraction in the carbonitride. Inserting the formulas of Narita [4] for the respective $K_{1\ldots4}$ results in the equation

$$\lg K = 3.40 - 8409/T \tag{9}$$

where solubility is only marginally influenced by −22/T due to regular solution enthalpy but more severely altered by 326/T due to the particle radius. A significant fraction of very small precipitates clearly enhances the solubility. The APT analysis on the present steels indicated particle sizes even below 2 nm. Hence, the use of an actual precipitate size distribution would provide a more accurate solubility product. By comparing the experimental solubility with that modelled by Eq. (9) in Fig. 7 it is obvious that both entropy and enthalpy terms deviate from

Table 4 – Solubility products calculated for the mixed (Nb,Ti)(C,N) with the formula $Nb_{0.76}Ti_{0.24}C_{0.89}N_{0.11}$ from Eq. (5).

Soaking temperature (°C)	Solubility product lg K	propagated error
950	−3.95	±0.66
1050	−3.19	±0.24
1100	−2.98	±0.21
1150	−2.86	±0.18
1200	−2.81	±0.17
1250	−2.79	±0.17

the experimentally derived solubility product. An activity change of C and N due to other alloying elements might produce the largest deviation of Eq. (9) vs. Eq. (6). Wagner interaction parameters of C and N with the main alloy elements Mn, Si, Cu and Ni have notable impact on the entropy term of the solubility product. For instance, the interaction of Mn with N decreases lg K by about 0.2 [12]. Comparing the measured solubility behavior against the one constructed for regular solution suggests that with progressing dissolution the composition of the particle changes from a more carbide-like to a more nitride-like character. It is also feasible that after nearly complete dissolution of Nb, remaining Ti and N could rearrange to form an insoluble TiN particle. The atom ratio of Ti:N is approximately 2:1 in the initial particle (Table 2), thus at least part of the Ti must have dissolved at the highest soaking temperature.

4.2. *Reflections on measurement accuracy and validity*

4.2.1. *Measurement accuracy of electrical resistivity and APT methods*

The electrical resistivity measurement in this study employed the so-called Kelvin or 4-terminal probe. The calculated propagated uncertainty of 0.2 nΩm is well reflected in the statistical uncertainty of the average values. If this value is scaled on the total change of electrical resistivity between 1250 °C and 950 °C (0.083 and 0.008 wt.-% Nb for Nb8+Ti), then the concentration uncertainty of the electrical resistivity method was below 0.003 wt.-% Nb. Larger sample aspect ratios will reduce this further as both voltage drop and length measurements increase relative to the measurement uncertainties.

Calibrating the indirect electrical resistivity method for the quantitative evaluation of complex Nb-Ti carbonitride dissolution using the direct APT method requires specific considerations related to the analyzed sampling volume. The electrical resistivity technique probes a material volume in the order of cubic centimeters whereas the APT technique is analyzing an extremely small material volume of around 10^{-4} μm^3. Thus, the first method averages over multiple grain dimensions while the latter method characterizes a highly localized condition within one individual grain. This could cause the observed discrepancy in the measured solute content especially for intermediate soaking conditions comprising partial dissolution of precipitates. Dissolving Nb atoms must diffuse away from the particle/matrix interface for producing a homogenous concentration profile across the entire grain area. The diffusion range of Nb and Ti for isothermal holding of 1800 s is displayed in Fig. 8 for the considered range of soaking temperatures. At 1100 °C the diffusion range of both microalloying atoms is in the order of only 4 μm. This means full homogenization of the dissolved atoms cannot be reached across an austenite grain which typically has sizes of 20–30 μm. Besides, the distribution of precipitates is not perfectly homogeneous as demonstrated by Fig. 5. Therefore, areas inside a grain and away from precipitates are expected having locally lower solute concentration. This effect can explain the observed difference between the APT and electrical resistivity methods especially at 1100 °C. Higher soaking temperatures increasingly enable homogenization of solute microalloys across the entire grain dimension. The diffusion range of Nb in austenite for a holding time of 1800 s at 950 °C is in the order of only 1.5 μm. However, the mean-free interparticle distance is calculated to be in the order of 0.8 μm if at least 90% of the precipitates present in the starting population (Fig. 2) remain undissolved at this temperature. Therefore, homogenization of dissolved

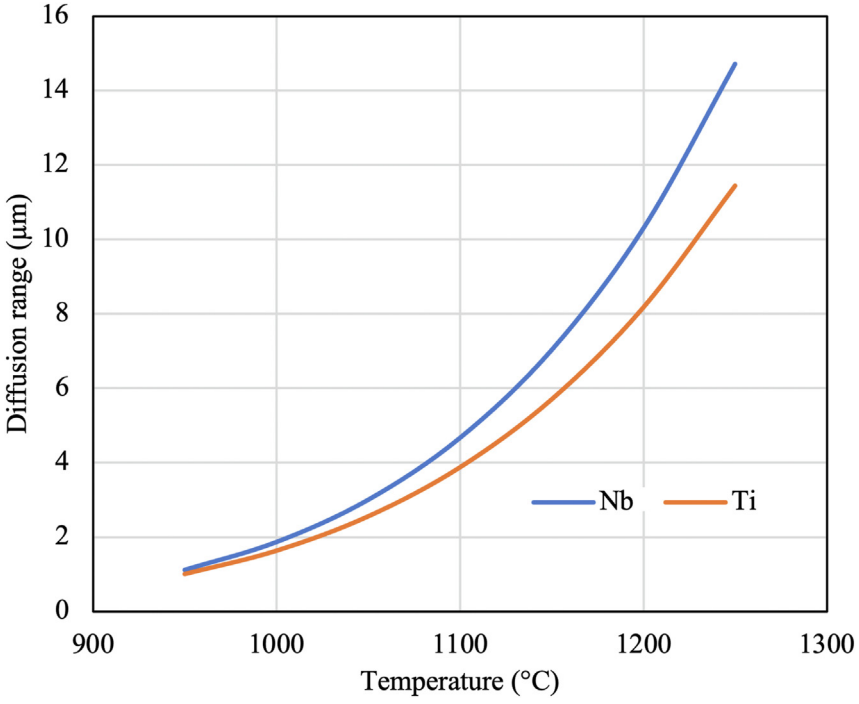

Fig. 8 – Calculated diffusion range of Nb and Ti as a function of austenite temperature for an isothermal holding duration of 1800 s. Nb and Ti diffusivity calculated according to Geise et al. [55] and Oikawa [56], respectively.

Nb between the particles is possible at the lowest soaking temperature and the APT analysis of the solute Nb level in the precipitate-free area can give a statistically correct result. This congruency of the solute Nb contents obtained by both methods for the lowest and highest soaking temperatures is also confirmed by Fig. 6. For the intermediate soaking temperature range, however, the electrical resistance method appears to give more accurate data for the solute content. Accordingly, the data originating from resistivity measurements provide the more reliable solubility product.

Regarding the error propagation of all uncertainties in the electrical measurements in the used setup, alloy Nb8+Ti showed relative resistivity increments sufficiently large to draw conclusions about the dissolution of Nb. Thus, this alloy provides the most suitable dataset for deriving the solubility product by a linear regression fit.

4.2.2. *Verification of resistivity measurements and related assumptions*

When deriving the solubility product according to Eq. (5), several assumptions were made. The average composition of particles analyzed by APT as shown in Table 2 was considered being representative for all precipitates since their individual compositions are not significantly deviating from the average. Figure 2 also revealed a size variation in the precipitate population of the as-cast sample. The particle size has a direct effect on the dissolution time and solubility [57]. Considering that the investigated particles, generally not being bigger than a few nanometers (Fig. 2), dissolve rather rapidly [58,59], equilibrium solubility should be reached over the duration of the current soaking treatments (1800 s). The observation that larger-sized precipitates contain a higher fraction of Ti suggests that significant amounts of solute Ti will only be present after soaking at higher temperatures when these precipitates dissolve to a larger degree.

The individual resistivity influences of Nb, Ti, C and N when dissolving complex carbonitride particles in the current steels cannot be separated from the total increase of electrical resistivity. Bohnekamp et al. [60] analyzed the individual electrical resistivity effects of various solutes in binary iron alloys, yet, a value for Nb has not been reported. However, quoted values for the electrical resistivity change caused by Nb(C,N) dissolution [23,24] are comparable to those found for the dissolution of complex Nb-Ti carbonitrides in the present investigation. Simoneau et al. [23] measured a resistivity change of in the range of 3–4 nΩm in steels containing 0.04 to 0.06 wt.-% Nb when heated from 900 to 1300 °C. Comparative measurements performed by the current authors on a Ti-free 0.085 wt.-% Nb-steel showed nearly the same resistivity change of $\Delta\rho \approx 5$ nΩm as in the Nb8+Ti steel. Therefore, the effect of solute Ti in the range of the current additions is considered being negligible. In congruency with literature [23,24], it can be concluded that the effect of solute Nb on the resistivity of the iron matrix is around 70 nΩm per wt.-% Nb.

The incremental change in electrical resistivity over the range of soaking temperatures, therefore, reflects the share of Nb dissolution. This share decreases towards higher austenite temperature and levels off when all niobium has been dissolved, which is well-reflected in the current resistivity measurements (Fig. 4a). The data of the Nb8+Ti steel indicated dissolution of 0.04 wt.-% Nb at a soaking temperature of 1050 °C. Accordingly, the incremental resistivity change of those steels containing not more than 0.04 wt.-% Nb (Nb2+Ti and Nb4+Ti) is levelling off at 1050 °C. The dissolution of Ti expected to occur at austenite temperatures above 1200 °C has only a small influence on the resistivity and cannot be reliably measured with the current measurement sensitivity.

5. Conclusions

The current study investigated the dissolution behavior of complex Nb-Ti carbonitride precipitates at austenite soaking temperatures in the range of 950–1250 °C for as-cast steel alloys with various Nb addition.

The composition of such precipitates was determined as $Nb_{0.76}Ti_{0.24}C_{0.89}N_{0.11}$ by APT measurements. The participating atoms appeared randomly distributed inside such particles according to the spatial resolution capability of the APT method.

The precise measurement of changes in the electrical resistance allowed the quantitative monitoring of niobium dissolution as a function of soaking temperature. It was found that solute Nb has a comparably strong effect on the electrical resistivity of the iron matrix which was determined to around 70 nΩm per wt.-% Nb. For the investigated steel containing 0.085 wt.-% Nb, the incremental resistivity change with progressing Nb dissolution was significantly larger than potential measurement uncertainties.

The electrical resistivity measurements were calibrated using the atom share of Nb determined by the APT method in the precipitate-free matrix. Eventual discrepancies between both methods are related to the small and highly localized sampling volume of APT that can reflect insufficient concentration homogenization of dissolved Nb at intermediate soaking temperatures. In that respect, a sufficiently optimized electrical resistivity method can give statistically more reliable results by integrating over a large sampling volume.

The dissolution behavior of the investigated 0.085 wt.-% Nb steel allowed deriving a novel solubility product for complex NbTi carbonitrides with random elemental distribution. Comparing the developed solubility product with those established for binary NbC and NbN indicated a transitional behavior from an initially more carbide-like towards a finally more nitride-like character when increasing the austenite soaking temperature. Despite the random arrangement of atoms in the initial particle, a theoretically calculated solubility product based on individual binary solubility products under the assumption of an ideal mixture was not congruent with the experimentally observed behavior. This confirms that with progressing dissolution, the composition of the particle changes towards a dominating nitride type, potentially leaving behind a TiN particle at highest soaking temperatures.

The higher temperature stability of such complex Nb-Ti carbonitrides as compared to binary compounds as well as their more homogeneous spatial distribution and smaller particle size as compared to primary TiN particles have an interesting potential for controlling the austenite grain size during slab soaking, welding, or high-temperature carburizing processes. The insights gained from the current study can also help designing microalloy compositions favoring the formation of such complex Nb-Ti carbonitrides.

Declaration of Competing Interest

The authors declare that they have no known competing financial interests or personal relationships that could have appeared to influence the work reported in this paper.

Acknowledgement

The authors J.W., D.B. and F.M. express their gratitude to Companhia Brasileira de Metalurgia e Mineração (CBMM) for providing the financial funding of this work. Furthermore, J.W., D.B. and F.M. would like to thank the Saarland State Chancellery for financial support within the ZuMat Project funded by the European Regional Development Fund (ERDF). The Atom Probe was financed by the Deutsche Forschungsgemeinschaft (DFG, German Research Foundation) and the Federal State Government of Saarland (INST 256/298-1 FUGG). We acknowledge support by DFG and Saarland University within the funding programme Open Access Publishing.

Appendix A. Supplementary data

Supplementary data to this article can be found online at https://doi.org/10.1016/j.jmrt.2022.03.098.

REFERENCES

[1] Gladman T. The Physical Metallurgy of Microalloyed Steels. London: The Institute of Materials; 1997.
[2] Turkdogan ET. Causes and effects of nitride and carbonitride precipitation during continuous casting. Iron Steelmak 1987;16:61–75.
[3] Irvine KJ, Pickering FB, Gladman T. Grain-refined C-Mn steels. Iron Steel Inst J 1967;205:161–82.
[4] Narita K. Physical chemistry of the groups IVa (Ti, Zr), Va (V, Nb, Ta) and the rare earth elements in steel. Trans Iron Steel Inst Jap 1975;15:145–52. https://doi.org/10.2355/isijinternational1966.15.145.
[5] Ma X, Miao C, Langelier B, Subramanian S. Suppression of strain-induced precipitation of NbC by epitaxial growth of NbC on pre-existing TiN in Nb-Ti microalloyed steel. Mater Des 2017;132:244–9. https://doi.org/10.1016/j.matdes.2017.07.006.
[6] Craven AJ, He K, Garvie LAJ, Baker TN. Complex heterogeneous precipitation in titanium–niobium microalloyed Al-killed HSLA steels—I.(Ti, Nb)(C, N) particles. Acta Mater 2000;48:3857–68. https://doi.org/10.1016/S1359-6454(00)00194-4.
[7] Solis-Bravo G, Merwin M, Garcia CI. Impact of precipitate morphology on the dissolution and grain-coarsening behavior of a Ti-Nb microalloyed linepipe steel. Metals 2020;10:89. https://doi.org/10.3390/met10010089.
[8] Zhang H, Xiong H. First-principles study of NbC heterogeneous nucleation on TiC vs . TiN in microalloy steel. Ironmak Steelmak 2020;47:77–83. https://doi.org/10.1080/03019233.2018.1483613.
[9] Hudd RC, Jones A, Kale M. Method for calculating the solubility and composition of carbonitride precipitates in steel with particular reference to niobium carbonitride. J Iron Steel Inst 1971;209:121–5.
[10] Hong SG, Kang KB, Park CG. Strain-induced precipitation of NbC in Nb and Nb–Ti microalloyed HSLA steels. Scripta Mater 2002;46:163–8. https://doi.org/10.1016/S1359-6462(01)01214-3.
[11] Eckstein H-J, Fennert M, Ohser J. Application of thermodynamic computations to the solution behaviour of niobium and vanadium carbonitrides. Steel Res 1993;64:143–7. https://doi.org/10.1002/srin.199300999.
[12] Sharma RC, Lakshmanan VK, Kirkaldy JS. Solubility of niobium carbide and niobium carbonitride in alloyed austenite and ferrite. Metall Trans A 1984;15:545–53. https://doi.org/10.1007/BF02644979.
[13] Siciliano F, Jonas J. Mathematical modeling of the hot strip rolling of Nb microalloyed steels. Metall Mater Trans 2000;31A:501–30.
[14] Webel J, Herges A, Britz D, Detemple E, Flaxa V, Mohrbacher H, et al. Tracing microalloy precipitation in Nb-Ti HSLA steel during austenite conditioning. Metals 2020;10:243. https://doi.org/10.3390/met10020243.
[15] Zhang Y, Miyamoto G, Furuhara T. Atom probe compositional analysis of interphase precipitated nano-sized alloy carbide in multiple microalloyed low-carbon steels. Microsc Microanal 2019;25:447–53. https://doi.org/10.1017/S1431927618015374.
[16] Okano G, Igarashi S, Ohno O, Yamamoto Y, Saito S, Oka Y. Determination of trace amounts of bismuth in steel by ICP-MS through a cascade-preconcentration and separation method. ISIJ Int 2015;55:332–4. https://doi.org/10.2355/isijinternational.55.332.
[17] Lu J, Omotoso O, Wiskel JB, Ivey DG, Henein H. Strengthening mechanisms and their relative contributions to the yield strength of microalloyed steels. Metall Mater Trans 2012;43:3043–61. https://doi.org/10.1007/s11661-012-1135-3.
[18] Hegetschweiler A, Staudt T, Kraus T. An improved method for the matrix dissolution extraction of nanoparticles from microalloyed steel. J Mater Sci 2019;54:5813–24. https://doi.org/10.1007/s10853-018-03263-0.
[19] Hegetschweiler A, Borovinskaya O, Staudt T, Kraus T. Single-particle mass spectrometry of titanium and niobium carbonitride precipitates in steels. Anal Chem 2019;91:943–50. https://doi.org/10.1021/acs.analchem.8b04012.
[20] Webel J, Weber L, Vardo E, Britz D, Kraus T, Mücklich F. Particle encapsulation techniques for atom probe tomography of precipitates in microalloyed steels. Ultramicroscopy 2021;223:113219. https://doi.org/10.1016/j.ultramic.2021.113219.
[21] Asano M, Masumura T, Tsuchiyama T, Takaki S, Takahashi J, Ushioda K. Quantitative evaluation of Cu particle dissolution in cold-worked ferritic steel. Scripta Mater 2017;140:18–22. https://doi.org/10.1016/j.scriptamat.2017.05.025.
[22] Masumura T, Taniguchi T, Uranaka S, Hirashima I, Tsuchiyama T, Maruyama N, et al. Estimation of solute carbon concentration by electrical resistivity measurement in martensitic steel. Tetsu-To-Hagane/Journal Iron Steel Inst. Japan. 2020;106:835–43. https://doi.org/10.2355/TETSUTOHAGANE.TETSU-2020-050.
[23] Simoneau R, Bégin G, Marquis AH. Progress of NbCN precipitation in HSLA steels as determined by electrical resistivity measurements. Met Sci 1978;12:381–6. https://doi.org/10.1179/msc.1978.12.8.381.
[24] Park JS, Lee YK. Determination of Nb(C,N) dissolution temperature by electrical resistivity measurement in a low-carbon microalloyed steel. Scripta Mater 2007;56:225–8. https://doi.org/10.1016/j.scriptamat.2006.10.007.

[25] Jung J-G, Park J-S, Kim J, Lee Y-K. Carbide precipitation kinetics in austenite of a Nb–Ti–V microalloyed steel. Mater Sci Eng 2011;528:5529–35. https://doi.org/10.1016/j.msea.2011.03.086.
[26] Maruyama N, Tabata S, Kawata H. Excess solute carbon and tetragonality in as-quenched Fe-1Mn-C (C:0.07 to 0.8 mass pct) martensite. Metall Mater Trans 2020;51:1085–97. https://doi.org/10.1007/s11661-019-05617-y.
[27] Garcia MP, Chen H, Eizadjou M, Lim B, Ringer SP, Barbaro FJ. Quantitative analysis of Nb in solid solution in low carbon steels by atom probe tomography and inductively coupled plasma mass spectroscopy. Mater Char 2021;179:111308. https://doi.org/10.1016/j.matchar.2021.111308.
[28] Palmiere EJ, Garcia CI, De Ardo AJ. Compositional and microstructural changes which attend reheating and grain coarsening in steels containing niobium. Metall Mater Trans 1994;25:277–86. https://doi.org/10.1007/BF02647973.
[29] Graux A, Cazottes S, Fabrègue D, Perez M, Danoix F. An alternative method for the measurement of precipitate volume fractions in microalloyed steels by the means of atom probe tomography. Mater Char 2020;164:110308. https://doi.org/10.1016/j.matchar.2020.110308.
[30] Felfer PJ, Killmore CR, Williams JG, Carpenter KR, Ringer SP, Cairney JM. A quantitative atom probe study of the Nb excess at prior austenite grain boundaries in a Nb microalloyed strip-cast steel. Acta Mater 2012;60:5049–55. https://doi.org/10.1016/j.actamat.2012.06.013.
[31] Wang HH, Tong Z, Wang J, Hodgson PD, Timokhina I. Study of Nb non-equilibrium segregation at prior austenite grain boundary in welding using atom probe tomography and modeling. J Mater Sci 2019;54:11320–7. https://doi.org/10.1007/s10853-019-03690-7.
[32] Deardo AJ. Niobium in modern steels. Int Mater Rev 2003;48:371–402. https://doi.org/10.1179/095066003225008833.
[33] Gault B, Moody MP, Cairney JM, Ringer SP. Atom Probe Microscopy. New York, NY: Springer New York; 2012. https://doi.org/10.1007/978-1-4614-3436-8.
[34] Thompson K, Lawrence D, Larson DJ, Olson JD, Kelly TF, Gorman B. In situ site-specific specimen preparation for atom probe tomography. Ultramicroscopy 2007;107:131–9. https://doi.org/10.1016/j.ultramic.2006.06.008.
[35] Gault B, Moody MP, Cairney JM, Ringer SP. Atom probe crystallography. Mater Today 2012;15:378–86. https://doi.org/10.1016/S1369-7021(12)70164-5.
[36] Vurpillot F, Bostel A, Blavette D. Trajectory overlaps and local magnification in three-dimensional atom probe. Appl Phys Lett 2000;76:3127–9. https://doi.org/10.1063/1.126545.
[37] Baker TN. Complex carbonitrides in multi-microalloyed Ti-containing HSLA steels and their influence on the mechanical properties. In: Titan. Technol. Microalloyed steels; 1994. p. 1997.
[38] Kunze J, Mickel C, Backmann G, Beyer B, Reibold M, Klinkenberg C. Precipitation of titanium nitride in low-alloyed steel during cooling and deformation. Steel Res 1997;68:441–9. https://doi.org/10.1002/srin.199700580.
[39] Zou H, Kirkaldy JS. Thermodynamic calculation and experimental verification of the carbonitride-austenite equilibrium in Ti-Nb microalloyed steels. Metall Trans A 1992;23:651–7. https://doi.org/10.1007/BF02801182.
[40] Arganda-Carreras I, Kaynig V, Rueden C, Eliceiri KW, Schindelin J, Cardona A, et al. Trainable Weka Segmentation: a machine learning tool for microscopy pixel classification. Bioinformatics 2017;33:2424–6. https://doi.org/10.1093/bioinformatics/btx180.
[41] Nöhrer M, Mayer W, Primig S, Zamberger S, Kozeschnik E, Leitner H. Influence of deformation on the precipitation behavior of Nb(CN) in austenite and ferrite. Metall Mater Trans 2014;45:4210–9. https://doi.org/10.1007/s11661-014-2373-3.
[42] Pereloma EV, Kostryzhev AG, AlShahrani A, Zhu C, Cairney JM, Killmore CR, et al. Effect of austenite deformation temperature on Nb clustering and precipitation in microalloyed steel. Scripta Mater 2014;75:74–7. https://doi.org/10.1016/j.scriptamat.2013.11.026.
[43] Timokhina I, Miller MK, Wang J, Beladi H, Cizek P, Hodgson PD. On the Ti-Mo-Fe-C atomic clustering during interphase precipitation in the Ti-Mo steel studied by advanced microscopic techniques. Mater Des 2016;111:222–9. https://doi.org/10.1016/j.matdes.2016.08.086.
[44] Kapoor M, O'Malley R, Thompson GB. Atom probe tomography study of multi-microalloyed carbide and carbo-nitride precipitates and the precipitation sequence in Nb-Ti HSLA steels. Metall Mater Trans 2016;47:1984–95. https://doi.org/10.1007/s11661-016-3398-6.
[45] Danoix F, Bémont E, Maugis P, Blavette D. Atom probe tomography I. Early stages of precipitation of NbC and NbN in ferritic steels. Adv Eng Mater 2006;8:1202–5. https://doi.org/10.1002/adem.200600225.
[46] Sha W, Chang L, Smith GDW, Cheng Liu, Mittemeijer EJ. Some aspects of atom-probe analysis of Fe-C and Fe-N systems. Surf Sci 1992;266:416–23. https://doi.org/10.1016/0039-6028(92)91055-G.
[47] Jessner P, Danoix R, Hannoyer B, Danoix F. Investigations of the nitrided subsurface layers of an Fe–Cr-model alloy. Ultramicroscopy 2009;109:530–4. https://doi.org/10.1016/j.ultramic.2008.11.028.
[48] Langelier B, Van Landeghem HP, Botton GA, Zurob HS. Interface segregation and nitrogen measurement in Fe–Mn–N steel by atom probe tomography. Microsc Microanal 2017;23:385–95. https://doi.org/10.1017/S1431927617000150.
[49] Li YJ, Ponge D, Choi P, Raabe D. Atomic scale investigation of non-equilibrium segregation of boron in a quenched Mo-free martensitic steel. Ultramicroscopy 2015;159:240–7. https://doi.org/10.1016/j.ultramic.2015.03.009.
[50] Stock J, Enloe CM, O'Malley RJ, Findley KO, Speer JG. Cooling rate effects on the as-cast titanium nitride precipitation size distribution in a low-carbon steel. AIST Trans 2014;11(No. 4):180–7.
[51] Zou H, Kirkaldy JS. Carbonitride precipitate growth in titanium/niobium microalloyed steels. Metall Trans A 1991;22:1511–24. https://doi.org/10.1007/BF02667365.
[52] Speer JG, Michael JR, Hansen SS. Carbonitride precipitation in niobium/vanadium microalloyed steels. Metall Trans 1987;18A:211–22.
[53] Costa e Silva A. Challenges and opportunities in thermodynamic and kinetic modeling microalloyed HSLA steels using computational thermodynamics. Calphad 2020;68:101720. https://doi.org/10.1016/j.calphad.2019.101720.
[54] Fujita N, Bhadeshia HKDH. Modelling precipitation of niobium carbide in austenite: multicomponent diffusion, capillarity, and coarsening. Mater Sci Technol 2001;17:403–8. https://doi.org/10.1179/026708301101510122.
[55] Geise J, Herzig C. Lattice and grain boundary diffusion of niobium in iron. Int J Mater Res 1985;76:622–6. https://doi.org/10.1515/ijmr-1985-760907.
[56] Oikawa H. Lattice diffusion in iron-A review. Tetsu-To-Hagane 1982;68:1489–97. https://doi.org/10.2355/tetsutohagane1955.68.10_1489.
[57] Porter DA, Easterling KE. Phase Transformations in Metals and Alloys. 2nd ed. CRC Press; 1992.
[58] Gong P, Palmiere EJ, Rainforth WM. Dissolution and precipitation behaviour in steels microalloyed with niobium during thermomechanical processing. Acta Mater 2015;97:392–403. https://doi.org/10.1016/j.actamat.2015.06.057.

[59] Mohrbacher H. Alloy design and processing strategies for grain coarsening-resistant carburizing steels. In: Int. Conf. Adv. Metall. Long Forged Prod. Proc. Association for Iron & Steel Technology; 2021. https://doi.org/10.33313/301/002.

[60] Bohnenkamp U, Sandström R. Evaluation of the electrical resistivity of steels. Steel Res 2000;71:410–6. https://doi.org/10.1002/srin.200001337.